New Journal of Physics
The open access journal at the forefront of physics

Deutsche Physikalische Gesellschaft DPG IOP Institute of Physics

PAPER • OPEN ACCESS

Modulation-induced long-range magnon bound states in one-dimensional optical lattices

To cite this article: Wenjie Liu *et al* 2020 *New J. Phys.* **22** 093052

New Journal of Physics
The open access journal at the forefront of physics

Deutsche Physikalische Gesellschaft DPG
IOP Institute of Physics

Published in partnership with: Deutsche Physikalische Gesellschaft and the Institute of Physics

OPEN ACCESS

RECEIVED
16 April 2020

REVISED
21 August 2020

ACCEPTED FOR PUBLICATION
26 August 2020

PUBLISHED
17 September 2020

PAPER

Modulation-induced long-range magnon bound states in one-dimensional optical lattices

Wenjie Liu[1,2], **Yongguan Ke**[1,3], **Bo Zhu**[1] and **Chaohong Lee**[1,2,4,5]

[1] Guangdong Provincial Key Laboratory of Quantum Metrology and Sensing & School of Physics and Astronomy, Sun Yat-Sen University (Zhuhai Campus), Zhuhai 519082, People's Republic of China
[2] State Key Laboratory of Optoelectronic Materials and Technologies, Sun Yat-Sen University (Guangzhou Campus), Guangzhou 510275, People's Republic of China
[3] Nonlinear Physics Centre, Research School of Physics, Australian National University, Canberra Australian Capital Territory 2601, Australia
[4] Synergetic Innovation Center for Quantum Effects and Applications, Hunan Normal University, Changsha 410081, People's Republic of China
[5] Author to whom any correspondence should be addressed.

E-mail: lichaoh2@mail.sysu.edu.cn

Keywords: ultracold atoms in optical lattices, magnon bound states, Floquet–Bloch band

Abstract

Magnon excitations play an important role in understanding quantum magnetism and magnon bound states observed with ultracold atoms in optical lattices. Here, we investigate how gradient magnetic field and periodically modulated spin-exchange strength affect the two-magnon excitations. In the Stark resonance where the driving frequency matches and smooths the potential bias, the system gains translational invariance in both space and time in the rotating frame, and thus we can develop a Floquet–Bloch band theory for two magnons. We find a new kind of bound states with relative distance no less than two sites, apart from the conventional bound states with relative distance at one site, which indicates the modulation-induced long-range interaction. We analytically derive an effective Hamiltonian via the many-body perturbation theory for a deeper understanding of such novel bound states and explore the interplay between these two types of bound states. Moreover, we propose to probe modulation-induced bound states via quantum walks. Our study not only provides a scheme to form long-range magnon bound states, but also lays a cornerstone for engineering exotic quantum states in multi-particle Floquet systems.

1. Introduction

In single-particle systems, periodic modulation not only provides a versatile tool to manipulate the quantum particles, but also brings novel states of matter into quantum systems. It has already been applied to control the hopping [1, 2], band structure [3, 4], and quantized transport of a single particle [5–8]. Remarkably, single-particle coherent destruction of tunneling [9, 10] and artificial gauge field [11] have been realized by well-designed modulation protocols. Recently, Floquet topological insulator of single particle has attracted considerable attentions in theoretical investigations [12–16] and has also been realized experimentally [17–19]. In principle, Floquet–Bloch theory of a single particle has been well developed to analyze the properties of periodically modulated systems [20]. However, many-body effects induced by time modulations are more challenging and appealing, such as collective emission of matter-wave jets [21], and discrete time crystals [22] etc.

It becomes possible to periodically modulate many-body systems with various methods in ultracold atomic systems. Modulation of particle–particle interaction may support many-body coherent destruction of tunneling [23], density-dependent correlated tunneling [24], density-dependent synthetic gauge fields [25], and effective three-body interactions [26]. Modulation of both on-site energy and interaction is a route to create the nearest-neighbour (NN) interaction and density-assisted tunneling [27]. Considering Hubbard-type models, periodic modulation of tunneling is used for engineering the interaction [28, 29].

Considering spin systems, periodically driven gradient magnetic field is supposed to tune a long-range interaction to a short-range interaction [30]. However, it is still unclear (i) how to tune a short-range interaction to a long-range interaction in a spin chain, (ii) what the engineered interaction brings to correlation properties of the states and (iii) how to probe the engineered interaction.

In this paper, we study two strongly interacting magnons in a spin-1/2 Heisenberg XXZ chain under a gradient magnetic field and periodic modulation of the spin-exchange strength, which may in principle be realized in one-dimensional spin-dependent optical lattices subjected to a gradient magnetic field. When the potential bias between NN sites is equal to the driving frequency, a single magnon can resonantly tunnel to the neighboring sites, called as Stark resonance. We develop a Floquet–Bloch band theory for two magnons, because the system in the rotating frame is invariant when the two magnons are shifted as a whole by multiples of lattice constant and time period. Apart from conventional bound states, we find that two magnons are bounded with a relative two-site distance by calculating the magnon–magnon correlation, indicating effective next-nearest-neighbour (NNN) interactions. An effective two-magnon model is obtained by using the many-body perturbation theory, which interprets the physical mechanism of modulation-induced long-range magnon bound states. The effective NNN interaction can be tuned to be positive or negative. When the NN interaction is equal to the modulation frequency, the NN interaction smooths the tilt in Floquet space and there exists a resonance between the bound states with relative one-site and two-site distances, called as interaction resonance. Considering the experimental realization, we also propose to probe the effective long-range magnon bound states via quantum walks.

2. Model

We consider ultracold two-level atoms in one-dimensional optical lattices. One can label the two hyperfine levels of atoms as spin up $|\uparrow\rangle$ and spin down $|\downarrow\rangle$. Through applying a gradient magnetic field, spin up and spin down feel opposite potentials at the lth site, $V_{l\uparrow} = -V_{l\downarrow} = lB$ with the gradient B. The Hamiltonian reads

$$\hat{H}_{\rm BH} = -\sum_{<l,g>,\sigma=\uparrow,\downarrow} t_\sigma \hat{b}^\dagger_{l\sigma}\hat{b}_{g\sigma} + \sum_{l\sigma}\frac{U_{\sigma\sigma}}{2}\hat{n}_{l\sigma}(\hat{n}_{l\sigma}-1) + U_{\uparrow\downarrow}\sum_l \hat{n}_{l\uparrow}\hat{n}_{l\downarrow} + \sum_{l\sigma} V_{l\sigma}\hat{n}_{l\sigma}. \tag{1}$$

Here, $\hat{b}^\dagger_{l\sigma}$ ($\hat{b}_{l\sigma}$) is the particle creation (annihilation) operator, $\hat{n}_{l\sigma}$ is the number operator, t_σ is the tunneling matrix element of $|\sigma\rangle$, and $U_{\sigma\sigma'}$ is the interaction between $|\sigma\rangle$ and $|\sigma'\rangle$. In the Mott-insulator regime with one boson per site, the Hamiltonian (1) can be mapped onto a Heisenberg XXZ chain,

$$\hat{H} = \sum_{l=1}^{L_{\rm t}}\left[J(t)\hat{S}^+_l\hat{S}^-_{l+1} + {\rm H.c.} + \Delta\hat{S}^z_l\hat{S}^z_{l+1} + lB\hat{S}^z_l\right] \tag{2}$$

with the total chain length $L_{\rm t}$. The spin-1/2 operators $\hat{S}^{\mathcal{I}}_l(\mathcal{I} = +, -, z)$ are defined as

$$\begin{aligned}\hat{S}^+_l &= \hat{b}^\dagger_{l\uparrow}\hat{b}_{l\downarrow},\\ \hat{S}^-_l &= \hat{b}^\dagger_{l\downarrow}\hat{b}_{l\uparrow},\\ \hat{S}^z_l &= (\hat{n}_{l\uparrow} - \hat{n}_{l\downarrow})/2,\end{aligned} \tag{3}$$

and the parameters yield

$$J = -\frac{2t_\uparrow t_\downarrow}{U_{\uparrow\downarrow}}, \qquad \Delta = -\frac{4t^2_\uparrow}{U_{\uparrow\uparrow}} - \frac{4t^2_\downarrow}{U_{\downarrow\downarrow}} + \frac{2(t^2_\uparrow + t^2_\downarrow)}{U_{\uparrow\downarrow}}. \tag{4}$$

Usually, the tunneling matrix elements of two spin components are $t_\sigma > 0$ in ultracold atomic experiments. J may be positive or negative by tuning attractive interaction ($U_{\uparrow\downarrow} < 0$) or repulsive interaction ($U_{\uparrow\downarrow} > 0$), respectively. Here, without loss of generality, we consider $J > 0$ and focus on the periodic modulation of spin-exchange strength,

$$J(t) = [J_0 + J_1\ \cos(\omega t)]/2 \tag{5}$$

with the DC amplitude J_0, the AC amplitude J_1 and the modulation frequency ω. For simplicity, we choose the units of $J_0 = \hbar = 1$.

Below we try to discuss the experimental possibilities of our time-modulated scheme, though great efforts are needed with state-of-art experimental techniques. To induce on-demand control, we consider two-level atoms in spin-dependent polarization-synthesized optical lattices described by $\mathcal{U}_\sigma(x,t) = \mathcal{U}^0_\sigma(t)\cos^2\{k[x - x_\sigma(t)]\}$ with a common wave vector k, lattice depths $\mathcal{U}^0_\sigma(t)$ and lattice positions $x_\sigma(t)$ for

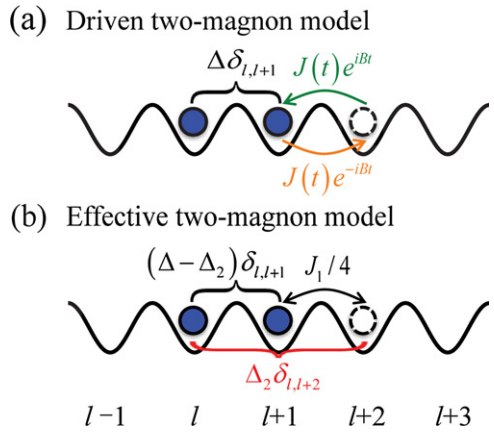

Figure 1. (a) The driven two-magnon model (6) with NN interaction and time-modulated hopping rate. (b) The effective two-magnon model (20) with the modulation-induced NNN interaction, modified NN interaction and reduced hopping rate.

$\sigma = \{\uparrow,\downarrow\}$ [31, 32]. Such optical lattices help to independently and separately modulate both lattice depths and lattice positions for the spin-up and spin-down atoms. In order to obtain the driving parameter $J(t)$, one may independently modulate $t_\downarrow$ by using an acousto-optic modulator to modulate the lattice depth for spin-down atoms satisfying $\mathcal{U}_\downarrow^0\,[1+\beta\ \cos(\omega t)]$ with the modulation depth β. At the same time, to fix Δ, one may tune the atom-atom interactions to satisfy $U_{\downarrow\downarrow} = 2U_{\uparrow\downarrow}$ via optical Feshbach resonance [33–36], that is, the Heisenberg spin interaction $\Delta = 2t_\uparrow^2(1/U_{\uparrow\downarrow} - 2/U_{\uparrow\uparrow})$ which is independent of $t_\downarrow(t)$. It may allow to further adjust this Heisenberg spin interaction Δ by controlling the tunneling rate $t_\uparrow$ for spin-up atoms.

Unlike the three-color modulations in the Fermi–Hubbard model [29], our Heisenberg XXZ chain (2) only involves a single frequency. The magnetic field gradient B breaks the translational symmetry of the system. When the modulation is off ($\omega = 0$), the ground state is the fully ferromagnetic state $|\downarrow\downarrow\downarrow\ldots\downarrow\rangle$ for a positive and sufficiently large B. By flipping spins over the ground state $|\downarrow\downarrow\downarrow\ldots\downarrow\rangle$, we obtain the excited states. Once one regards the ground state $|\downarrow\downarrow\downarrow\ldots\downarrow\rangle$ as a vacuum state, magnon can be regarded as the basic excitation around the ferromagnetic ground state. Considering the mapping relations $|\downarrow\rangle \leftrightarrow |0\rangle, |\uparrow\rangle \leftrightarrow |1\rangle$, $\hat{S}_l^+ \leftrightarrow \hat{a}_l^\dagger, \hat{S}_l^- \leftrightarrow \hat{a}_l$, and $\hat{S}_l^z \leftrightarrow \hat{n}_l - \frac{1}{2}$, it amounts to load magnons into the tilted optical lattice with periodically driven hopping rate and NN interaction, i.e., $\hat{H} = \sum_l \left[J(t)\hat{a}_l^\dagger\hat{a}_{l+1} + \text{H.c.} + \Delta\hat{n}_l\hat{n}_{l+1} + Bl\hat{n}_l\right]$. $\hat{a}_l^\dagger$ ($\hat{a}_l$) creates (annihilates) a magnon at site l and satisfies the commutation relations of the hard-core bosons. $\hat{n}_l = \hat{a}_l^\dagger\hat{a}_l$ is the number operator.

By a unitary treatment $\hat{H}' = \hat{U}\hat{H}\hat{U}^\dagger - i\hat{U}\frac{\partial}{\partial t}\hat{U}^\dagger$ with $\hat{U} = \exp(\mathrm{i}\sum_l lBt\hat{n}_l)$ [37, 38], the driven magnon Hamiltonian in the rotating frame is given by,

$$\hat{H}' = \sum_{l=1}^{L_t}\left[J(t)\mathrm{e}^{-\mathrm{i}Bt}\hat{a}_l^\dagger\hat{a}_{l+1} + \text{H.c.}\right] + \Delta\sum_{l=1}^{L_t}\hat{n}_l\hat{n}_{l+1}. \tag{6}$$

If we impose periodic boundary condition, Hamiltonian (6) preserves translational invariance, which is slightly different from Hamiltonian (2) at the boundary. We only consider the bulk properties where the tiny difference between Hamiltonian (2) and Hamiltonian (6) takes no effect. For convenience, we focus on Hamiltonian (6) with periodic boundary condition in the following paper.

Since $[\hat{H}', \hat{n}] = 0$ with $\hat{n} = \sum_l \hat{n}_l$, the total magnon number is conserved. This means that subspaces with different magnon numbers are decoupled. To take magnon–magnon interaction into account, two-magnon excitations are fundamental objects and give enlightenment to multi-magnon excitations. We aim to manipulate a NNN two-magnon bound state and explore its interplay with the original NN bound state from both numerical and analytical perspectives. Based upon a two-body ansatz related to center-of-mass and relative positions, we concentrate our analysis on the subspace of two-magnon excitations. The driven two-magnon model is schematically shown in figure 1(a).

In the absence of the gradient magnetic field and periodic driving ($B = J_1 = 0$), the spin-1/2 XXZ chain occurs a quantum phase transition at $\Delta = J$. For a two-magnon system, an isolated bound-state band and a continuum scattering-state band appear in the energy spectrum for $\Delta > J$, while the bound-state band merges into the continuum one for $0 < \Delta < J$. After flipping two spins over the ground state with all spins downward, two magnons undergo Bloch oscillations in the presence of the gradient magnetic field [39]. In our paper, we only consider the Stark resonance, i.e., $\omega = B$, where photon-assisted tunneling resonances may happen [40, 41].

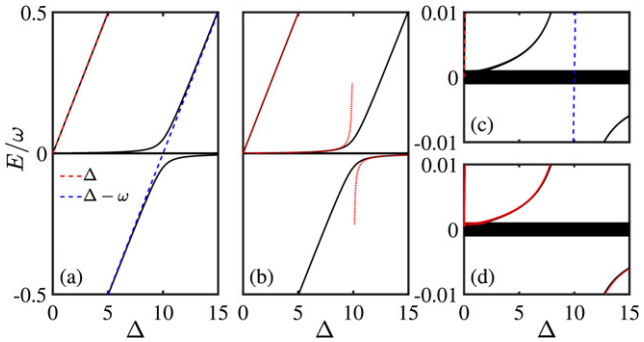

Figure 2. (a) Quasienergy spectrum E as a function of Δ given by the static effective Hamiltonian $\hat{H}_{\rm F}$ (black solid lines). The red and blue dashed lines respectively represent $E = \Delta$ and $E = \Delta - \omega$. (b) The quasienergy spectra obtained by the Floquet–Bloch lattice model (13) (black solid lines) for $F = 5$ and the effective two-magnon model (20) (red dotted lines). (c) and (d) The enlarged quasienergy spectra around scattering-state bands in (a) and (b), respectively. The other parameters are chosen as $\omega = B = 10, J_0 = 1, J_1 = 0.01$ and $L_{\rm t} = 21$.

3. Floquet spectrum analysis

Only NN antiferromagnetic interaction ($\Delta > 0$) is considered in the Hamiltonian (6), while our conclusions can easily be extended to the corresponding ferromagnetic one ($\Delta < 0$) due to the related symmetry analysis [39]. The interplay between the NN interaction and time modulation makes it possible to induce long-range magnon bound states. To understand how the long-range magnon bound states come from, we need to analyze the Floquet spectrum and the Floquet states. We aim to study the modulation-induced NNN magnon bound state and give an effective picture for its coexistence and competition with the original NN magnon bound state. However, in addition to the NNN magnon bound states, our system can also be modulated to induce other bound states. In appendix, we give a brief discussion on the modulation-induced magnon bound states with relative distances at three and four sites.

The driven two-magnon Hamiltonian (6) satisfies a discrete time translation symmetry $\hat{H}(t+T) = \hat{H}(t)$ with a Floquet period $T = 2\pi/\omega$. $\hat{\mathcal{T}}$ is the time-ordering operator, and we can define a time-evolution operator in one period as

$$\hat{U}_T = \hat{\mathcal{T}} \exp(-\mathrm{i}\int_0^T \hat{H}'(t)\mathrm{d}t) \equiv \exp(-\mathrm{i}\hat{H}_{\rm F}T), \tag{7}$$

where the static effective Hamiltonian

$$\hat{H}_{\rm F} = \frac{i}{T}\ \log \hat{U}_T \tag{8}$$

governs the dynamics at stroboscopic times nT ($n = 1, 2, 3, \ldots$. Before analyzing the dynamics, it is helpful to solve the eigenvalue problem, $\hat{H}_{\rm F}|u_n\rangle = E_n|u_n\rangle$, where E_n and $|u_n\rangle$ are quasienergy and Floquet state, respectively. E_n can be restricted in the interval $[-\omega/2, \omega/2]$, which we term as the first Floquet–Brillouin zone. The quasienergy has a period ω and consists of replicas of that in the first Floquet–Brillouin zone. We calculate the quasienergy spectrum as a function of the NN interaction regarding the static effective Hamiltonian (8), as shown in figure 2(a). The other parameters are chosen as $\omega = B = 10, J_0 = 1, J_1 = 0.01$ and $L_{\rm t} = 21$. There is a continuum flat band around zero energy, with eigenstates regarded as the scattering states. When $J_0, J_1 \ll \Delta$, two magnons at the NN sites approximate the bound states with energy $\sim \Delta$. The red dashed line $E = \Delta$ is added in figure 2(a), which is well fitting with an isolated band (black solid lines) corresponding to bound states with relative distance as one site. It becomes clear that $E = \Delta - \omega$ (blue dashed line) is the replica of $E = \Delta$ (red dashed line). Around the interaction resonance $\Delta - \omega = 0$, the bound-state band $E = \Delta - \omega$ (blue dashed line) seriously departs from two isolated bands (black solid lines). Thus, the two isolated bands (black solid lines) around $\Delta - \omega \approx 0$ must be a modulation-induced effect.

The arbitrary two-magnon states can be expanded as $|\Psi\rangle = \sum_{l_1<l_2}\psi_{l_1l_2}|l_1l_2\rangle$, with probability amplitudes $\psi_{l_1l_2} = \langle\mathbf{0}|\hat{a}_{l_2}\hat{a}_{l_1}|\Psi\rangle$ for one magnon at the l_1th site and the other at the l_2th site. After substituting the two-magnon state in the Fock basis into the Schrödinger equation

$$i\frac{\mathrm{d}}{\mathrm{d}t}|\Psi(t)\rangle = \hat{H}'|\Psi(t)\rangle, \tag{9}$$

the probability amplitudes $\psi_{l_1l_2}(t)$ at instantaneous time t satisfy

$$i\frac{\partial}{\partial t}\psi_{l_1l_2}(t) = M(t)\left(\psi_{l_1,l_2+1}(t) + \psi_{l_1+1,l_2}(t)\right) + M^*(t)\left(\psi_{l_1,l_2-1}(t) + \psi_{l_1-1,l_2}(t)\right) + \Delta\delta_{l_1,l_2\pm1}\psi_{l_1l_2}(t) \tag{10}$$

with $M(t) = J_1/4 + J_0/2e^{-i\omega t} + J_1/4e^{-i2\omega t}$. Considering the periodic boundary condition, we have $\psi_{l_1,l_2+L_t} = \psi_{l_1+L_t,l_2} = \psi_{l_1,l_2}$. Due to the time periodicity, we can express the probability amplitudes $\psi_{l_1l_2}(t)$ by the Fourier components $\psi_{l_1l_2}(t) = e^{-iEt}\sum_{\chi=-\infty}^{\infty} e^{-i\chi\omega t}U_{l_1,l_2,\chi}$ [2, 20]. Then we have

$$|\Psi(t)\rangle = e^{-iEt}\sum_{l_1<l_2,\chi} e^{-i\chi\omega t}U_{l_1,l_2,\chi}|l_1,l_2,\chi\rangle \tag{11}$$

where $|U_{l_1,l_2,\chi}|^2$ is the probability distributing in the state $|l_1,l_2,\chi\rangle$. χ is the Floquet index taking values from $-\infty$ to ∞. The state $|l_1,l_2,\chi\rangle$ intuitively represents two particles living in real space and Floquet space. Due to the particle conservation, the two particles always share a common χ, that is, the two particles transfer from χ to χ' as a bounded pair. Replacing the state (11) into the equation (9) and averaging it over one period, we can obtain

$$EU_{l_1,l_2,\chi} = (\Delta\delta_{l_1,l_2\pm1} - \chi\omega)U_{l_1,l_2,\chi} + \sum_q \mathcal{J}_q\left(U_{l_1,l_2+1,\chi-q} + U_{l_1+1,l_2,\chi-q}U_{l_1,l_2-1,\chi+q} + U_{l_1-1,l_2,\chi+q}\right) \tag{12}$$

with $q = 0, 1, 2$, $\mathcal{J}_0 = \mathcal{J}_2 = J_1/4$ and $\mathcal{J}_1 = J_0/2$. It is equal to a Floquet–Bloch lattice model,

$$\hat{H}_{\rm FB} = \hat{H}^0_{\rm FB} + \hat{H}^1_{\rm FB}, \tag{13}$$

with

$$\hat{H}^0_{\rm FB} = \sum_{l_1,l_2,\chi}\left(\Delta\delta_{l_1,l_2\pm1} - \chi\omega\right)|l_1,l_2,\chi\rangle\langle l_1,l_2,\chi| \tag{14}$$

and

$$\hat{H}^1_{\rm FB} = \sum_{l_1,l_2,\chi,q}\left(\mathcal{J}_q|l_1,l_2,\chi\rangle\langle l_1,l_2+1,\chi-q| + \text{H.c.}\right) + \sum_{l_1,l_2,\chi,q}\left(\mathcal{J}_q|l_1,l_2,\chi\rangle\langle l_1+1,l_2,\chi-q| + \text{H.c.}\right) \tag{15}$$

with $q = 0, 1, 2$. We establish an equivalence between a periodically driven two-magnon model (6) and the Floquet–Bloch lattice model (13). The motion of two magnons in the periodically driven one-dimensional lattice in figure 1(a) is equivalent to the time-independent hopping dynamics of two magnons in a two-dimensional lattice model with a potential energy gradient along the χ direction. Here, $\hat{H}^0_{\rm FB}$ consists of the NN interaction and the gradient potential $-\chi\omega$ along χ direction. $\hat{H}^1_{\rm FB}$ consists of individual hopping of magnons in the same χ and pair-hopping between χ and χ' with $\chi' = \chi \pm 1, \chi \pm 2$.

Numerically, we can calculate the quasienergy spectrum by truncating the Floquet spaces ranging from $\chi = -f$ to f, and the total truncation number $F = 2f + 1$. In the high-frequency case, $\omega \gg J_0, J_1$, the energy barrier between χ and $\chi \pm 1$ is so large that the two magnons tend to localize at a few χ. A small truncation number gives sufficiently exact results and enables us to apply the perturbation theory to obtain an effective Hamiltonian. However, as the modulation frequency decreases, the wave function becomes spread over a larger range of χ, and a larger truncation number is needed. By choosing the same parameters as figure 2(a) and $F = 5$, and diagonalizing the Floquet–Bloch lattice model (13), we also give the quasienergy spectrum as a function of Δ, see black solid lines in figure 2(b). Compared the quasienergy spectrum obtained by $\hat{H}_{\rm F}$ in figure 2(a) with the one obtained by $\hat{H}_{\rm FB}$ in figure 2(b), they are almost the same. Based on the above Floquet analysis, we will investigate the Bloch states under a periodic boundary condition far away from and around the interaction resonance.

4. Two-body Floquet–Bloch band

In this section, we obtain the two-body Floquet–Bloch band, a significant analysis of the many-body Bloch theorem to the periodically modulated system. Based on the Floquet–Bloch lattice model (13) which has cotranslational symmetry along the real space but violates such symmetry along the Floquet space due to the effective gradient potential $-\chi\omega$, we can apply the many-body Bloch theorem in the real space and leave alone the Floquet index χ. Away from the interaction resonance $\Delta - \omega = 0$, we analyze the isolated Floquet–Bloch bands and reveal the modulation-induced long-range two-magnon bound states. Such process can also be perfectly captured by an effective Hamiltonian via the many-body perturbation theory. Near the interaction resonance, we find the hybrid of two kinds of magnon bound states.

4.1. Modulation-induced long-range two-magnon bound states

Imposing periodic boundary condition, the Floquet–Bloch lattice model (13) is invariant by shifting the two magnons as a whole in the real space. Naturally, we introduce the center-of-mass and relative positions $R = (l_1 + l_2)/2$ and $r = l_1 - l_2$, respectively. The center-of-mass quasimomentum K is a conserved quantity.

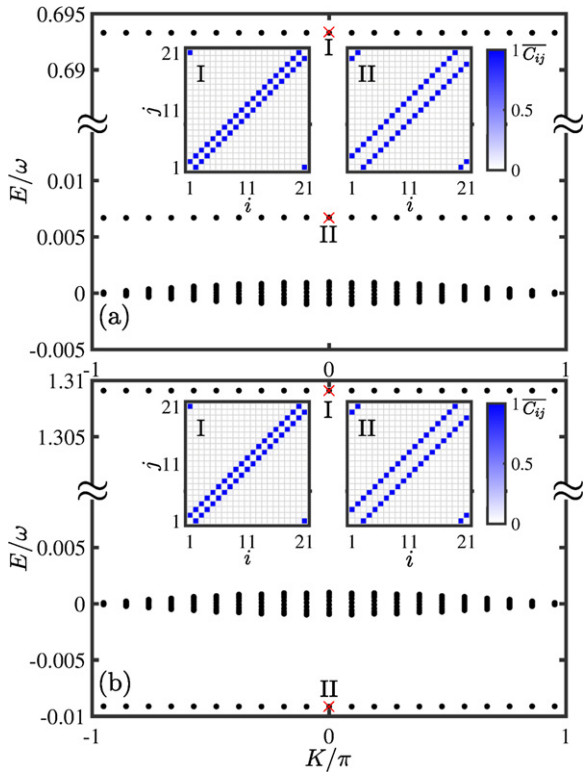

Figure 3. Quasienergy spectrum E vs center-of-mass momentum K away from the interaction resonance for (a) $\Delta-\omega=-3$ and (b) $\Delta-\omega=3$. The insets I and II respectively describe the normalized magnon–magnon correlations $\overline{C_{ij}}=C_{ij}/C_{ij}^{\max}$ of Floquet states labeled in the isolated bands. The Floquet space is truncated to be $\chi=0,\pm1,\pm2$. The other parameters are chosen as $\omega=B=10, J_0=1, J_1=0.01$ and $L_t=21$.

According to the many-body Bloch theorem, the wave-function is a Bloch wave along the coordinate of center-of-mass position, i.e., $U_{l_1,l_2,\chi}=e^{iKR}\phi_\chi(r)$ where $\phi_\chi(r)$ is the amplitude depending on the relative position r and the Floquet position χ.

Substituting the above ansatz into equation (13), the amplitude $\phi_\chi(r)$ satisfies the following eigenequation in the quasimomentum space,

$$E\phi_\chi(r)=\sum_q \mathcal{J}_q^K\left(\phi_{\chi-q}(r-1)+\phi_{\chi-q}(r+1)\right)+\left(\Delta\delta_{r,\pm1}-\chi\omega\right)\phi_\chi(r) \tag{16}$$

with $q=0,\pm1,\pm2$, $\mathcal{J}_0^K=J_1/2\ \ cos(K/2)$, $\mathcal{J}_{\pm1}^K=J_0/2e^{\pm iK/2}$ and $\mathcal{J}_{\pm2}^K=J_1/4e^{\pm iK/2}$. Under the periodic boundary condition, we find $e^{iKL_t}=1$ and $\phi_\chi(r+L_t)=e^{iKL_t/2}\phi_\chi(r)$ with $K=2\pi\alpha/L_t$ for $\alpha=-L,-L+1,\ldots,L$. Here the total chain length is $L_t=2L+1$. Moreover, since the magnons are hard-core bosons, we have $\phi_\chi(0)=0$ and $\phi_\chi(r)=\phi_\chi(-r)$.

Solving the above eigenequation (16), we can obtain the two-body Floquet–Bloch bands vs K in figure 3 (more results for longer-range magnon bound states are shown in appendix). Δ is chosen at the left- and right-hand sides of the interaction resonance as $\Delta=7,13$ for figures 3(a) and (b), respectively. The other parameters are chosen as $\omega=B=10, J_0=1, J_1=0.01$ and $L_t=21$. The Floquet space is truncated to be $\chi=0,\pm1,\pm2$. At the left-hand side of the interaction resonance, there are two isolated bands above a continuum band which ranges from $-|J_1|$ to $|J_1|$, as shown in figure 3(a). This is qualitatively different from a conventional two-band energy spectrum of two-magnon excitations in NN interaction quantum spin chains without the periodic driving. In figure 3(a), an extra band appears in between the continuum band and NN-interaction bound-state band, with quite a similar structure to the bound-state band arising from the NN interaction. While at the right-hand side of the interaction resonance, the two isolated bands sandwich the continuum band, as shown in figure 3(b). It will be clear later that the difference between figures 3(a) and (b) is related to the positive and negative values of the effective interaction. A suitable choice of parameters results in a negative modulation-induced bound band below the continuum band.

To better understand the band structure, it is instructive to calculate the magnon–magnon correlations of corresponding Floquet states labeled with I and II in figure 3. The magnon–magnon correlation is defined as $C_{ij}=\langle\Psi(T)|\hat{a}_i^\dagger\hat{a}_j^\dagger\hat{a}_j\hat{a}_i|\Psi(T)\rangle$ where $|\Psi(T)\rangle$ is the Floquet state with a given quasimomentum K. i and j take values from 1 to L_t. The magnon–magnon correlations at two specific lines $i=j\pm d$ in the (i,j)

plane serve as a sensitive evidence of the two-magnon bound states, where d depends on the specific magnon–magnon interactions. For example, due to the NN interaction, the Floquet states marked with I are well distributed among the minor-diagonal lines $i = j \pm 1$ of the magnon–magnon correlations in the insets I of figure 3. While for the Floquet states marked with II, the insets II of figure 3 show the magnon–magnon correlations are mainly distributed in the next-minor-diagonal lines. The type-II Floquet state indicates the existence of effective long-range magnon bound states. The correlation properties of the other Floquet states in these two bands are similar to their Floquet states with quasimomentum $K = 0$. They are characteristic signatures of two types of bound-state bands, respectively derived from the NN interaction and NNN interaction. Thus, we can claim the existence of modulation-induced long-range magnon bound states.

4.2. Effective two-magnon model

Below particular attention is paid to attain an effective two-magnon model for understanding and interpreting the origination of the modulation-induced long-range magnon bound states. Given the perturbation conditions $|\Delta - \omega| \gg J_0/2$ and $|\Delta - 2\omega| \gg J_1/4$, we divide the Floquet–Bloch lattice model (13) into two parts, $\hat{H}^0_{\rm FB}$ as a dominating term and $\hat{H}^1_{\rm FB}$ as a perturbation term. In the high-frequency region, $\omega \gg J_0, J_1$, it is sufficient to just take into account five χ with $\chi = 0, \pm 1, \pm 2$. The dominating term $\hat{H}^0_{\rm FB}$ is separated into two subspaces. The first subspace includes two kinds of states: (i) the states $\{|l, l+1, 0\rangle\}$ with $1 \leqslant l \leqslant L_{\rm t}$ and $E = \Delta$, (ii) the states $\{|l_1, l_2, 0\rangle\}$ with $l_1 \neq l_2 - 1, 1 \leqslant l_1 < l_2 \leqslant L_{\rm t}$ and $E = 0$. The complementary subspace consists of (iii) the states $\{|l, l+1, \chi\rangle\}$ with $1 \leqslant l \leqslant L_{\rm t}$ and $E = \Delta - \chi\omega$, (iv) the states $\{|l_1, l_2, \chi\rangle\}$ with $l_1 \neq l_2 \pm 1, 1 \leqslant l_1 < l_2 \leqslant L_{\rm t}$ and $E = -\chi\omega$ for $\chi = \pm 1, \pm 2$. We project the Floquet–Bloch lattice model (13) onto the first subspace with $\chi = 0$ to obtain the effective two-magnon model $\hat{H}_{\rm Eff} = \hat{h}_0 + \hat{h}_1 + \hat{h}_2$ via a perturbative expansion up to the second order. In the lowest order and first order, we have

$$\hat{h}_0 = \Delta \sum_l |l, l+1, 0\rangle\langle l, l+1, 0| \tag{17}$$

and

$$\hat{h}_1 = \frac{J_1}{4} \sum_{l_1 l_2} \left(|l_1, l_2, 0\rangle \left(\langle l_1, l_2 + 1, 0| + \langle l_1 + 1, l_2, 0| \right) + \text{H.c.} \right), \tag{18}$$

which respectively retain the original NN interaction Δ and NN tunneling in $\chi = 0$. The second-order effective Hamiltonian reads

$$\hat{h}_2 = -\Delta_2 \sum_l \left(|l, l+1, 0\rangle\langle l, l+1, 0| - |l, l+2, 0\rangle\langle l, l+2, 0| \right) \tag{19}$$

with $\Delta_2 = J_0^2 \Delta/[2(\omega^2 - \Delta^2)] + J_1^2 \Delta/[8(4\omega^2 - \Delta^2)]$. Interestingly, the second-order process not only contributes to the NNN interaction, but modifies the original NN interaction. Since the high-order term is much smaller than the second-order one in the perturbation parameter region, it allows us to ignore the results beyond the second-order term.

By means of the perturbation theory [42, 43], the effective two-magnon model up to second order in $\chi = 0$ is given as

$$\hat{H}_{\rm Eff} = \sum_l \left[\frac{J_1}{4} \hat{a}_l^\dagger \hat{a}_{l+1} + \text{H.c.} + (\Delta - \Delta_2) \hat{n}_l \hat{n}_{l+1} + \Delta_2 \hat{n}_l \hat{n}_{l+2} \right]. \tag{20}$$

$\sum_l \hat{n}_l = 2$ restricts $\hat{H}_{\rm Eff}$ to the two-magnon sector. The effective two-magnon model (20) can be schematically described in figure 1(b) with the renormalized parameters. The effective NNN interaction comes from the asymmetric pathways between absorbing and consequently emitting phonons, $\{|l_2 - l_1 = 2, 0\rangle \to |l_2 - l_1 = 1, +\chi\rangle \to |l_2 - l_1 = 2, 0\rangle, \chi \neq 0\}$ and the inverse process, $\{|l_2 - l_1 = 2, 0\rangle \to |l_2 - l_1 = 1, -\chi\rangle \to |l_2 - l_1 = 2, 0\rangle, \chi \neq 0\}$. This is the origin of NNN interactions in a periodically modulated interacting system. Coherent destruction of tunneling is a phenomenon in which the effective tunneling rate is zero due to the destructive interference of different paths. Coherent destruction of tunneling is possible to occur when one utilizes a driving field to switch off the tunneling [23]. Under the zero effective tunneling rate, particles keep frozen at the initial positions in the time evolution. The renormalized tunneling rate is reduced to a constant $J_1/4$ for our effective two-magnon model (20), which indicates there is no signal of coherent destruction of tunneling in our system with the parameters we focus on. Therefore, two magnons of our system are allowed to undergo the tunneling dynamics. Note that modulation amplitude J_1 determines the width of the continuum band $[-|J_1|, |J_1|]$. Once J_1 is sufficiently large, the NNN-interaction bound-state band may be not enough to completely separate from the continuum band. With the effective two-magnon model (20), we can systematically create and control the

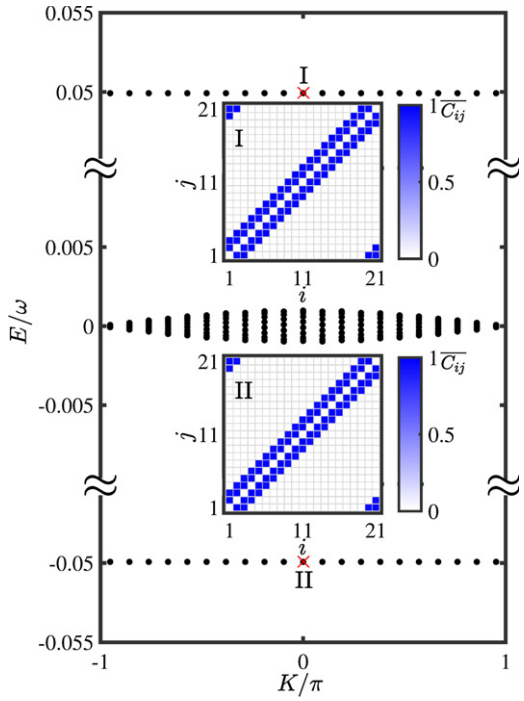

Figure 4. Quasienergy spectrum E vs K with the interaction resonance $\Delta = \omega$. The insets I and II respectively describe the normalized magnon–magnon correlations $\overline{C_{ij}} = C_{ij}/C_{ij}^{\max}$ of Floquet states labeled in the top and bottom bands in the quasienergy spectrum. The Floquet space is truncated to be $\chi = 0, \pm 1, \pm 2$. The other parameters are chosen as $\omega = B = 10$, $J_0 = 1, J_1 = 0.01$ and $L_t = 21$.

NNN interaction. The long-range two-magnon bound states arising from the modulation-induced NNN interaction constitute the central idea of our paper.

To show the concreteness, we compare the quasienergy spectrum given by the effective two-magnon model (20) and that given by the Floquet–Bloch lattice model (13), respectively see the red dotted and black solid lines in figure 2(b). It is clear that the isolated bands are well consistent in the perturbation parameter regime $|\Delta - \omega| \gg J_0/2$ and $|\Delta - 2\omega| \gg J_1/4$. The perturbation conditions mean the energy gap between the above two subspaces $\chi = 0$ and $\chi = \pm 1, \pm 2$ of $\hat{H}^0_{\rm FB}$ should be much larger than their tunneling rate. This energy gap decreases as Δ approaches to ω, so that the perturbation condition is no longer satisfied and the effective two-magnon model (20) is invalid. As shown in figure 2(b) (red dotted lines), the isolated bound band of $\hat{H}_{\rm Eff}$ is no longer fitting with the modulation-induced band of $\hat{H}_{\rm FB}$ when the NN interaction Δ approaches to the modulation frequency ω. But their continuum bands are always well consistent. In order to clearly clarify the modulation-induced bound band, we just plot the continuum band of $\hat{H}_{\rm FB}$ in figure 2(b).

4.3. Resonance between two types of bound states

However, the effective two-magnon model (20) becomes invalid around the interaction resonance $\Delta = \omega$ where the NN interaction smooths the tilt in Floquet space. To understand what happens under the interaction resonance, we calculate the band structure and magnon–magnon correlations via the Floquet spectrum analysis based on the eigenequation (16) (see figure 4). The truncated Floquet space is limited in $\chi = 0, \pm 1, \pm 2$.

For $\hat{H}^0_{\rm FB}$, its eigenstates $\{|l, l+1, \chi\rangle : 1 \leqslant l \leqslant L_t\}$ with $E_0 = \Delta - \chi\omega$ and $\{|l_1, l_2, \chi - 1\rangle : l_1 \neq l_2 - 1, 1 \leqslant l_1 < l_2 \leqslant L_t\}$ with $E_0 = -(\chi - 1)\omega$ become degenerate with the energy E_0 and the energy difference $\Delta - \omega = 0$. Once $\hat{H}^1_{\rm FB}$ is added, this energy degeneracy will be broken, and these states are not longer eigenstates of the full Hamiltonian (13). Two types of bound states $|l_2 - l_1 = 1, \chi\rangle$ and $|l_2 - l_1 = 2, \chi - 1\rangle$ are coupled by a first-order process with the tunneling rate $J_0/2$, while state $|l_2 - l_1 = 1, \chi\rangle$ couples state $\{|l_2 - l_1 > 2, \chi - 1\rangle : l_1 \neq l_2 - 1, l_2 - 2\}$ by a second-order or even higher-order term, which can be neglected in the high-frequency region. Here we are able to just consider the first-order tunneling process between two types of bound states $|l, l+1, \chi\rangle$ and $|l, l+2, \chi - 1\rangle$, then the corresponding states of the system (13) can be written as a superposition $(|l, l+1, \chi\rangle \pm |l, l+2, \chi - 1\rangle)/\sqrt{2}$ and the corresponding energies are $E = E_0 \pm J_0/2$.

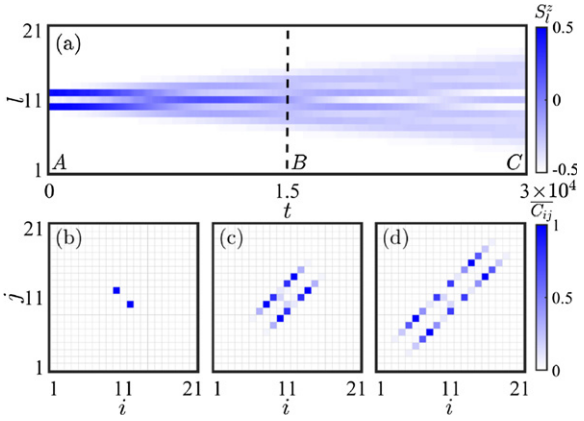

Figure 5. Quantum walks of two magnons in the driven Heisenberg XXZ chain under a gradient magnetic field (2). (a) is the time evolution of spin distributions $S_l^z(t)$. (b)–(d) are the normalized magnon–magnon correlations $\overline{C_{ij}} = C_{ij}/C_{ij}^{\max}$ for different moments marked as A, B and C in (a). At the initial moment A ($t = 0$), two magnons are prepared in $|10, 12\rangle$, so one can see two points in (10, 12) and (12, 10) in (b). (c) and (d) reveal that, in the course of the time evolution, two magnons mainly move along the next-minor-diagonal lines of the magnon–magnon correlation. The other parameters are chosen as $\Delta = 7$, $\omega = B = 10, J_0 = 1, J_1 = 0.01$ and $L_t = 21$.

Now we focus on the first Floquet–Brillouin zone $E \in [-\omega/2, \omega/2]$, the energies of bound states $|1\rangle = |l, l+1, 1\rangle$ and $|2\rangle = |l, l+2, 0\rangle$ are $E_0 = 0$. Once the coupling between $|1\rangle$ and $|2\rangle$ turns on with strength $J_0/2$, the eigenstates follow $|\pm\rangle = (|1\rangle \pm |2\rangle)/\sqrt{2}$ and eigenvalues are $E_0 \pm J_0/2$. The energy bands at the top and bottom are almost symmetrical with respect to $E_0 = 0$, and the energy gap is J_0 (see figure 4). The parameters are chosen as $J_0 = 1, J_1 = 0.01, \Delta = \omega = B = 10$ and $L_t = 21$, in the high-frequency region $\omega \gg J_0, J_1$. We respectively mark the two Floquet states as I and II in the quasienergy spectrum and analyze their correlated properties in the insets I and II of figure 4. The top and bottom bands behave almost the same, that is, the magnon–magnon correlation is basically equal probability distribution on the minor-diagonal and next-minor-diagonal lines. These numerical results completely follow the related theoretical analysis.

There exists a process in which, with the increasing of Δ, a bound-state band caused by the NNN interaction in $\chi = 0$ emerges from the continuum band. When Δ approaches to ω, it gradually mixes with the bound-state band caused by the NN interaction in $\chi = 1$. The NN-interaction bound-state band in $\chi = 1$ plays a dominant role when Δ is large enough. Similarly, with the increasing of Δ, an isolated NN-interaction bound-state band in $\chi = 1$ appears below the continuum band, is mixed with the NNN-interaction one in $\chi = 0$ around the interaction resonance $\Delta = \omega$, and finally turns to the one of the NNN interaction in $\chi = 0$ for a sufficiently large Δ.

5. Probing long-range two-magnon bound states

Two-magnon quantum walks may provide an excellent method to probe the modulation-induced long-range two-magnon bound states. The dynamics of single magnon and two-magnon bound states in an undriven spin chain have been observed in ultracold atomic experiments [44, 45]. It is worth numerically simulating the dynamics of two strongly correlated magnons, initially localizing on the sites $l_1 = 10$ and $l_2 = 12$, which can be prepared by flipping two NNN spins from a saturated ferromagnetic state with all spins downward $|\downarrow\downarrow\ldots\downarrow\rangle$. To investigate the dynamics of magnons initially locating in the bulk of the spin chain, we resort to numerically solve the time-dependent Schrödinger equation. Starting from the driven spin-1/2 Heisenberg XXZ chain under a gradient magnetic field (2), the time evolution of an arbitrary two-magnon state $|\psi(t)\rangle$ obeys the Schrödinger equation $i\frac{\mathrm{d}}{\mathrm{d}t}|\psi(t)\rangle = \hat{H}|\psi(t)\rangle$, where $|\psi(t)\rangle = \sum_{l_1<l_2}\psi_{l_1 l_2}(t)|l_1 l_2\rangle$ and the probability amplitudes $\psi_{l_1 l_2}(t) = \langle \mathbf{0}|\hat{S}_{l_2}^{-}\hat{S}_{l_1}^{-}|\psi(t)\rangle$. With the instantaneous wave function $|\psi(t)\rangle$, we trace out the time-dependent spin distributions $S_l^z(t) = \langle\psi(t)|\hat{S}_l^z|\psi(t)\rangle$ and the instantaneous magnon–magnon correlations $C_{ij}(t) = \langle\psi(t)|\hat{S}_i^{+}\hat{S}_j^{+}\hat{S}_j^{-}\hat{S}_i^{-}|\psi(t)\rangle$ for different moments, where l, i and j take values from 1 to L_t.

Figure 5 displays the time evolution of spin distributions and the corresponding instantaneous magnon–magnon correlations at three different moments for $\Delta = 7, \omega = B = 10, J_0 = 1, J_1 = 0.01$ and $L_t = 21$. Figure 5(a) shows a light cone in the time evolution of spin distributions before the two magnons collide with the boundaries. We timely cut off the evolution of spin distributions to avoid the boundary effects and analyze its magnon–magnon correlations, marking A, B and C in figure 5(a). As shown in

figures 5(b)–(d), almost all of the magnons are distributed among the next-minor-diagonal lines in the magnon–magnon correlation. These results follow from the circumstance that two strongly NNN interacting magnons initially occupying the NNN sites form a bound pair and tunnel together on the spin chain. These time evolved results are in agreement with our analytical predictions. The two-magnon quantum walks may pave the way for verifying the modulation-induced long-range magnon bound states in experiments.

6. Summary and discussion

We have presented a scheme for generating tunable long-range magnon bound states by introducing a gradient magnetic field and time-modulated spin-exchange into the spin-1/2 Heisenberg XXZ chain. Desired long-range magnon bound states can be engineered by changing the modulated parameters and the interaction Δ. The prerequisite lies in the modulation frequency ω is equal to the magnetic field gradient B, which enables a single magnon to tunnel resonantly onto its neighbors. It can be understood as the photon-assisted tunneling among the spin chain. We not only analyze the correlation properties of modulation-induced long-range magnon bound states, but also explore the interplay between the original bound state and modulation-induced bound state as NN interaction changes. Further, we obtain an effective two-magnon model via a many-body perturbation theory to interpret the origin and condition for the remarkable long-range magnon bound states. The effective two-magnon model becomes invalid near the interaction resonance $\Delta = \omega$, where resonance between the two types of bound states happens. In addition, two-magnon quantum walks may be used as an experimental verification of modulation-induced long-range magnon bound states. Our scheme is not limited to two-magnon systems, and also gives insights into engineering novel states of matter of multi-particle Floquet systems.

A few promising questions remain open and motivate further investigations. For example, this proposed scheme has potential to realize the fractional topological states which exist in the one-dimensional superlattice with the dipole–dipole interactions [46]. By introducing the modulation-induced NNN interaction, the competitive relation between two kinds of bound states may bring different topological effects into periodically modulated NN-interaction spin chains. In the whole text, we focus on the analysis in the high-frequency region, while more abundant phenomena may arise in the low-frequency region.

Acknowledgments

This work is supported by the Key-Area Research and Development Program of GuangDong Province under Grants No. 2019B030330001, the National Natural Science Foundation of China (NNSFC) under Grants [No. 11874434, No. 11574405], and the Science and Technology Program of Guangzhou (China) under Grants No. 201904020024. YK is partially supported by the Office of China Postdoctoral Council (Grant No. 20180052), the National Natural Science Foundation of China (Grant No. 11904419), and the Australian Research Council (DP200101168).

Appendix. Longer-range bound states

Our system not only is able to induce NNN bound states, but also has potential to engineer longer-range bound states. In figure A1, we show how the quasienergy spectrum changes with J_0 obtained by the Floquet–Bloch lattice model (13) for $F = 15$. The other parameters are chosen as $\omega = B = 1$, $\Delta = 0.7$, $J_0 = 1.2$, $J_1 = 0.001$ and $L_t = 21$. With the increase of J_0, more and more modulation-induced bands emerge. To illustrate how the longer-range bound state is induced, we take $J_0 = 1.2$ marked with red dashed line in figure A2 as an example. We obtain the two-body Floquet–Bloch bands versus K by solving the eigenequation (16) in figure A2. Four isolated bands appear above the continuum band in figure A2. We respectively mark the Floquet states from different isolated bands as I, II, III and IV in the quasienergy spectrum and analyze their correlated properties in the insets I, II, III and IV of figure A2. The magnon–magnon correlations clearly show that, aside from NN and NNN bound states, the bound states with relative distance at three and four sites appear. It is worth noting that these correlations mostly distribute along their corresponding diagonal lines and partly distribute in other diagonal lines, called as hybridization. According to our further numerical results, in the appearance of modulation-induced longer-range bound state, hybridization inevitably arises and even more complex case, e.g., the transformation between different types of bound states in the same bound-state band.

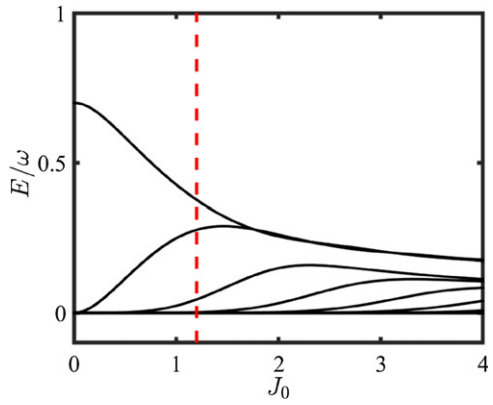

Figure A1. Quasienergy spectrum E vs J_0 obtained by the Floquet–Bloch lattice model (13) for $F = 15$. The other parameters are chosen as $\omega = B = 1$, $\Delta = 0.7$, $J_1 = 0.001$ and $L_t = 21$. The red dashed line corresponds to $J_0 = 1.2$.

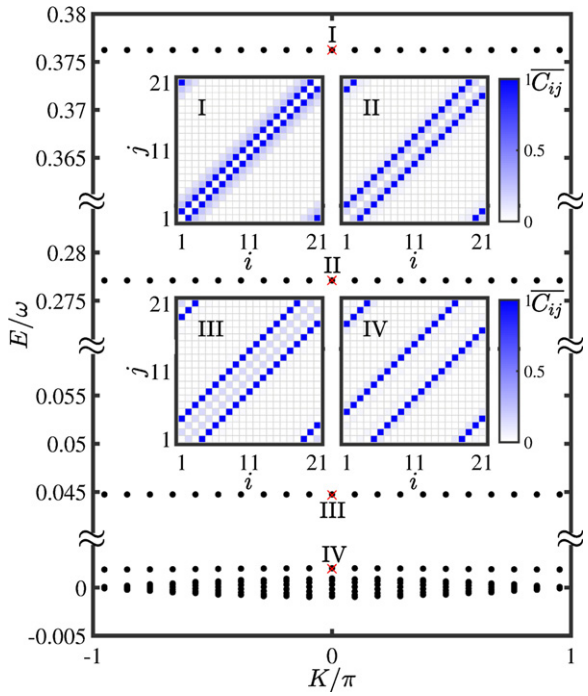

Figure A2. Quasienergy spectrum E vs K by solving the eigenequation (16) for $F = 15$. The insets I, II, III and IV respectively describe the normalized magnon–magnon correlations $\overline{C_{ij}} = C_{ij}/C_{ij}^{\max}$ of Floquet states labeled in the four bound-state bands above the continuum band. The other parameters are chosen as $\omega = B = 1$, $\Delta = 0.7$, $J_0 = 1.2$, $J_1 = 0.001$ and $L_t = 21$.

References

[1] Dal Lago V, Atala M and Foa Torres L E F 2015 Floquet topological transitions in a driven one-dimensional topological insulator *Phys. Rev.* A **92** 023624

[2] Zhu B, Zhong H, Ke Y, Qin X, Sukhorukov A A, Kivshar Y S and Lee C 2018 Topological Floquet edge states in periodically curved waveguides *Phys. Rev.* A **98** 013855

[3] Zheng W and Zhai H 2014 Floquet topological states in shaking optical lattices *Phys. Rev.* A **89** 061603

[4] Holthaus M 2015 Floquet engineering with quasienergy bands of periodically driven optical lattices *J. Phys. B: At. Mol. Opt. Phys.* **49** 013001

[5] Lohse M, Schweizer C, Zilberberg O, Aidelsburger M and Bloch I 2016 A Thouless quantum pump with ultracold bosonic atoms in an optical superlattice *Nat. Phys.* **12** 350

[6] Nakajima S, Tomita T, Taie S, Ichinose T, Ozawa H, Wang L, Troyer M and Takahashi Y 2016 Topological Thouless pumping of ultracold fermions *Nat. Phys.* **12** 296

[7] Zilberberg O, Huang S, Guglielmon J, Wang M, Chen K P, Kraus Y E and Rechtsman M C 2018 Photonic topological boundary pumping as a probe of 4D quantum Hall physics *Nature* **553** 59

[8] Lohse M, Schweizer C, Price H M, Zilberberg O and Bloch I 2018 Exploring 4D quantum Hall physics with a 2D topological charge pump *Nature* **553** 55
[9] Grossmann F, Dittrich T, Jung P and Hänggi P 1991 Coherent destruction of tunneling *Phys. Rev. Lett.* **67** 516
[10] Grossmann F and Hänggi P 1992 Localization in a driven two-level dynamics *Europhys. Lett.* **18** 571
[11] Goldman N and Dalibard J 2014 Periodically driven quantum systems: effective Hamiltonians and engineered Gauge fields *Phys. Rev.* X **4** 031027
[12] Oka T and Aoki H 2009 Photovoltaic Hall effect in graphene *Phys. Rev.* B **79** 081406
[13] Kitagawa T, Berg E, Rudner M and Demler E 2010 Topological characterization of periodically driven quantum systems *Phys. Rev.* B **82** 235114
[14] Ho D Y H and Gong J 2014 Topological effects in chiral symmetric driven systems *Phys. Rev.* B **90** 195419
[15] Zhou L, Wang H, Ho D Y H and Gong J 2014 Aspects of Floquet bands and topological phase transitions in a continuously driven superlattice *Eur. Phys. J.* B **87** 204
[16] Rudner M S and Lindner N H 2019 Floquet topological insulators: from band structure engineering to novel non-equilibrium quantum phenomena (arXiv:1909.02008)
[17] Wang Y H, Steinberg H, Jarillo-Herrero P and Gedik N 2013 Observation of Floquet–Bloch states on the surface of a topological insulator *Science* **342** 453
[18] Rechtsman M C, Zeuner J M, Plotnik Y, Lumer Y, Podolsky D, Dreisow F, Nolte S, Segev M and Szameit A 2013 Photonic Floquet topological insulators *Nature* **496** 196
[19] Jotzu G, Messer M, Desbuquois R, Lebrat M, Uehlinger T, Greif D and Esslinger T 2014 Experimental realization of the topological Haldane model with ultracold fermions *Nature* **515** 237
[20] Gomez-Leon A and Platero G 2013 Floquet–Bloch theory and topology in periodically driven lattices *Phys. Rev. Lett.* **110** 200403
[21] Clark L W, Gaj A, Feng L and Chin C 2017 Collective emission of matter-wave jets from driven Bose–Einstein condensates *Nature* **551** 356
[22] Sacha K and Zakrzewski J 2017 Time crystals: a review *Rep. Prog. Phys.* **81** 016401
[23] Gong J, Morales-Molina L and Hänggi P 2009 Many-body coherent destruction of tunneling *Phys. Rev. Lett.* **103** 133002
[24] Meinert F, Mark M J, Lauber K, Daley A J and Nägerl H-C 2016 Floquet engineering of correlated tunneling in the Bose–Hubbard model with ultracold atoms *Phys. Rev. Lett.* **116** 205301
[25] Clark L W, Anderson B M, Feng L, Gaj A, Levin K and Chin C 2018 Observation of density-dependent Gauge fields in a Bose–Einstein condensate based on micromotion control in a shaken two-dimensional lattice *Phys. Rev. Lett.* **121** 030402
[26] Lee C, Ho W, Yang B, Gong J and Papić Z 2018 Floquet mechanism for non-abelian fractional quantum Hall states *Phys. Rev. Lett.* **121** 237401
[27] Zhao Z, Knolle J and Mintert F 2019 Engineered nearest-neighbor interactions with doubly modulated optical lattices *Phys. Rev.* A **100** 053610
[28] Anisimovas E, Žlabys G, Anderson B M, Juzeliūnas G and Eckardt A 2015 Role of real-space micromotion for bosonic and fermionic Floquet fractional Chern insulators *Phys. Rev.* B **91** 245135
[29] Cardarelli L, Greschner S and Santos L 2016 Engineering interactions and anyon statistics by multicolor lattice-depth modulations *Phys. Rev.* A **94** 023615
[30] Lee T 2016 Floquet engineering from long-range to short-range interactions *Phys. Rev.* A **94** 040701
[31] Robens C, Zopes J, Alt W, Brakhane S, Meschede D and Alberti A 2017 Low-entropy states of neutral atoms in polarization-synthesized optical lattices *Phys. Rev. Lett.* **118** 065302
[32] Robens C, Brakhane S, Alt W, Meschede D, Zopes J and Alberti A 2018 Fast, high-precision optical polarization synthesizer for ultracold-atom experiments *Phys. Rev. Appl.* **9** 034016
[33] Fedichev P O, Kagan Y, Shlyapnikov G V and Walraven J T M 1996 Influence of nearly resonant light on the scattering length in low-temperature atomic gases *Phys. Rev. Lett.* **77** 2913
[34] Theis M, Thalhammer G, Winkler K, Hellwig M, Ruff G, Grimm R and Denschlag J H 2004 Tuning the scattering length with an optically induced Feshbach resonance *Phys. Rev. Lett.* **93** 123001
[35] Blatt S, Nicholson T L, Bloom B J, Williams J R, Thomsen J W, Julienne P S and Ye J 2011 Measurement of optical Feshbach resonances in an ideal gas *Phys. Rev. Lett.* **107** 073202
[36] Nicholson T L, Blatt S, Bloom B J, Williams J R, Thomsen J W and Ye J 2015 Optical Feshbach resonances: field-dressed theory and comparison with experiments *Phys. Rev.* A **92** 022709
[37] Buchleitner A and Kolovsky A R 2003 Interaction-induced decoherence of atomic Bloch oscillations *Phys. Rev. Lett.* **91** 253002
[38] Kolovsky A and Buchleitner A 2003 Floquet–Bloch operator for the Bose–Hubbard model with static field *Phys. Rev.* E **68** 056213
[39] Liu W, Ke Y, Zhang L and Lee C 2019 Bloch oscillations of multimagnon excitations in a Heisenberg XXZ chain *Phys. Rev.* A **99** 063614
[40] Teichmann N, Esmann M and Weiss C 2009 Fractional photon-assisted tunneling for Bose–Einstein condensates in a double well *Phys. Rev.* A **79** 063620
[41] Ma R, Tai M E, Preiss P M, Bakr W S, Simon J and Greiner M 2011 Photon-assisted tunneling in a biased strongly correlated Bose gas *Phys. Rev. Lett.* **107** 095301
[42] Bravyi S, DiVincenzo D P and Loss D 2011 Schrieffer–Wolff transformation for quantum many-body systems *Ann. Phys., NY* **326** 2793
[43] Takahashi M 1977 Half-filled Hubbard model at low temperature *J. Phys. C: Solid State Phys.* **10** 1289
[44] Fukuhara T *et al* 2013 Quantum dynamics of a mobile spin impurity *Nat. Phys.* **9** 235
[45] Fukuhara T, Schauß P, Endres M, Hild S, Cheneau M, Bloch I and Gross C 2013 Microscopic observation of magnon bound states and their dynamics *Nature* **502** 76
[46] Xu Z, Li L and Chen S 2013 Fractional topological states of dipolar fermions in one-dimensional optical superlattices *Phys. Rev. Lett.* **110** 215301